THE UNIVERSITY OF WARWICK

For more information, please contact the WRAP Team at: publications@warwick.ac.uk

warwickpublicationswrap

highlight your research

http://wrap.warwick.ac.uk/

FORMULATION AND OPTIMIZATION OF THE
ENERGY-BASED BLENDED QUASICONTINUUM METHOD

M. LUSKIN, C. ORTNER, AND B. VAN KOTEN

ABSTRACT. We formulate an energy-based atomistic-to-continuum coupling method based on blending the quasicontinuum method [14] for the simulation of crystal defects. We present optimal choices of approximation parameters (blending function and finite element grid) and confirm our analytical predictions in numerical tests.

1. INTRODUCTION

A major goal of materials science is to predict the macroscopic properties of materials from their microscopic structure. For this purpose, it is necessary to understand the behavior of defects in these materials. We propose a computational tool, the energy-based blended quasicontinuum method (BQCE), for understanding defects such as cracks, dislocations, vacancies, and interstitials in crystalline materials.

Accurate modeling of the region near a defect requires the use of computationally expensive atomistic models. Such models are practical only for small problems. However, a defect may interact with a large region of the material through long-range elastic fields. Thus, accurate simulation of defects requires the use of a large computational domain; typically, the size required rules out the use of atomistic models for the entire region of interest.

Fortunately, the long-range elastic fields generated by a defect are well described by continuum models which can be efficiently computed using the finite-element method. Thus, defects can be accurately and efficiently simulated by coupled models which use an atomistic model near the defect and a continuum model elsewhere. We call any such model an *atomistic-to-continuum coupling*.

Many atomistic-to-continuum couplings have been proposed in recent years [1–3, 8, 11, 14, 19, 21]; see [13, 22] for a survey of atomistic-to-continuum couplings and computational benchmark tests. These couplings fall into two major classes: energy-based and force-based. Energy-based couplings provide an approximation to the atomistic energy of a configuration of atoms. Force-based couplings provide a non-conservative force-field which approximates the forces on each atom under the atomistic model. Our BQCE method is an energy-based coupling. Both types of

couplings have intrinsic advantages; the development of energy-based couplings is especially important for finite-temperature applications since equilibrium statistical properties and transition rates can be directly approximated [5, 12].

The primary source of error for most energy-based couplings is the *ghost force*. We say that a coupling suffers from ghost forces if it predicts non-zero forces on the atoms in a perfect lattice. Although many attempts have been made to develop an energy-based coupling free from ghost forces such couplings are currently known only for a limited range of problems [6, 18, 19, 21].

Shapeev's method [19] applies to one and two-dimensional simple crystals with an atomistic energy based on a pair interaction model, and can be extended to 3D if a modified "continuum model" is used [20]. GR-AC was proposed in [6, 21], and has recently been implemented for a two dimensional crystal with nearest neighbor multi-body interactions in [18]. No ghost force free methods are currently known for three-dimensional crystals, for multi-lattice crystals (except in 1D [15]), or for atomistic models with general multi-body interactions. The field-based coupling of Iyer and Gavini [11] is another interesting approach; however, it is unlear at present whether it is competitive in terms of computational complexity and generality.

In our BQCE method, the ghost forces cannot be eliminated but can be controlled in terms of an additional approximation parameter (the blending width). BQCE applies to a wide range of problems for which no ghost force free methods are known; these problems include three-dimensional crystals with general multi-body interactions as well as multi-lattices. We believe that BQCE is an attractive method for such challenging and physically important problems.

The key feature of BQCE is a *blending region* where the atomistic and continuum contributions to the total energy are smoothly mixed. The ghost forces of the BQCE method can be made arbitrarily small by increasing the size of this blending region. BQCE shares the idea of a blending region with the bridging domain method [3], the AtC coupling [1], and the Arlequin method [2]. By contrast, the energy-based quasicontinuum method (QCE) [14], Shapeev's method [19], and GR-AC [6, 18, 21] exhibit an abrupt transition between the atomistic and continuum models. We call any method with a blending region a *blended method*, and we call the weights which mix the atomistic and continuum contributions to the energy a *blending function*.

Both the bridging domain method and AtC coupling are very general formulations, each of them incorporating BQCE and QCE as special cases. Our BQCE formulation provides a set of specific instructions for the successful implementation of a blended method. We identify two important practical differences between BQCE and the bridging domain and AtC coupling methods. First, the BQCE method specifies a strong coupling between the atomistic and continuum regions, whereas weak couplings based on Lagrange multipliers or the penalty method have been used in most work involving the bridging domain and AtC coupling methods. Second, in BQCE, we blend the atomistic site-energy with a continuum site-energy based on the continuum site-energy defined in some formulations of the QCE method (see Section 3). This guarantees that BQCE correctly predicts the total energy of a perfect lattice subjected to uniform strain.

Our approach to blending is supported by rigorous analysis. In [23], we showed that the ghost force error of BQCE in 1D does indeed decrease with the size of the blending region, and we found that the error is minimized when the blending function is a cubic-spline. We also found that the error of the BQCE method in

predicting lattice instabilities can be reduced by increasing the size of the blending region.

More recently, we have shown similar consistency results in higher dimensions [17]. We have conjectured error estimates based on these consistency results, and we use our conjectured estimates to derive complexity estimates which bound the error of the BQCE method in terms of the number of degrees of freedom used in the simulation. We then use these complexity estimates to derive optimal approximation parameters for the BQCE method [17]. Implementation of BQCE requires the choice of two approximation parameters: a *blending function* β and a finite-element mesh $\mathcal{T}$ which is used to compute the continuum contribution to the energy. In Section 4.3, we give optimal choices of β and $\mathcal{T}$ for the problem of a point defect in a 2D crystal.

In the present work, we demonstrate the validity of our analysis in a computational test problem in which we simulate a micro-crack in a two-dimensional crystal (see Figure 1). In Section 4, we give a precise formulation of BQCE for simple lattices with a general multi-body interaction model. We will present a formulation of BQCE for multi-lattice crystals in a forthcoming work [17]. In Section 4.3, we offer advice on choosing the blending function β and the mesh $\mathcal{T}$ based on our analysis in [17]. The results of this analysis are summarized in Table 4.3.

In Section 5, we describe the details of our numerical experiment. We use an atomistic energy based on the Embedded Atom Method. We did not choose our atomistic energy to model any specific physical material; instead, the atomistic energy is a toy model chosen for its simplicity. Finally, we present the results of our experiment in Section 5.3. The observed rates of convergence are in agreement with the rates predicted in Section 4.3. In particular, the error of BQCE in the $W^{1,2}$ semi-norm decreases as $\mathrm{DoF}^{-\frac{1}{2}}$ where DoF is the number of degrees of freedom.

2. The Atomistic Energy

Let Λ be a d-dimensional Bravais lattice. We call Λ the *reference lattice*, and we refer to points $\xi \in \Lambda$ as *atoms*. Let

$$\mathscr{Y} := \{y : \Lambda \to \mathbb{R}^d; y(\xi) \neq y(\eta) \text{ for all } \xi \neq \eta\}$$

be the set of *deformations* of Λ. Let $\Omega_{\mathrm{a}} \subset \Lambda$ be a finite subset of Λ. We call Ω_{a} the *atomistic computational domain*.

In the Embedded Atom Method (EAM), the energy of Ω_{a} subjected to deformation y takes the form

$$(2.1) \qquad \mathcal{E}^{\mathrm{a}}(y) := \sum_{\xi \in \Omega_{\mathrm{a}}} \left\{ \sum_{\substack{\eta \in \Lambda \\ \eta \neq \xi}} \frac{1}{2} \phi\big(|y(\eta) - y(\xi)|\big) + G\bigg(\sum_{\substack{\eta \in \Lambda \\ \eta \neq \xi}} \rho\big(|y(\eta) - y(\xi)|\big) \bigg) \right\},$$

where ϕ is a pair potential, ρ is an electron density function, and G is an embedding function. We call the inner sum

$$(2.2) \qquad \mathcal{E}^{\mathrm{a}}_{\xi}(y) := \sum_{\substack{\eta \in \Lambda \\ \eta \neq \xi}} \frac{1}{2} \phi\big(|y(\eta) - y(\xi)|\big) + G\bigg(\sum_{\substack{\eta \in \Lambda \\ \eta \neq \xi}} \rho\big(|y(\eta) - y(\xi)|\big) \bigg)$$

the *atomistic site-energy of atom ξ*. We observe that the sum defining the energy of an atom is finite in practice even though summation ranges over the infinite lattice

Λ. This is because the pair potential ϕ and electron density function ρ are taken to have a *cut-off radius* r_c such that

$$\phi(r) = \rho(r) = 0 \text{ for all } r \geq r_c.$$

When defining the Blended Quasicontinuum Energy (BQCE), we will consider a more general class of potentials than EAM. Roughly speaking, we will require only that the total energy can be decomposed into a sum of localized site-energies associated with each atom. By *localized*, we mean that the energy associated with an atom ξ does not depend on the positions of atoms beyond a certain cut-off distance. Such an assumption may be violated for certain energies arising from quantum mechanics, but does hold for most empirical potentials including EAM, the bond-angle potentials, and so forth. In addition, we require that the site-energies are *homogeneous*; that is, the energies of atoms which have the same local environment are the same.

To make these assumptions precise, we let $\mathcal{E}_\xi^a(y)$ denote the site-energy associated with atom ξ under deformation y and require that it is of the form

$$(2.3) \qquad \mathcal{E}_\xi^a(y) := V\left(\left\{y(\eta) - y(\xi) : \eta \in \Lambda \setminus \{\xi\}, |y(\eta) - y(\xi)| \leq r_c\right\}\right),$$

where V the site-energy potential. We assume that the resulting site-energies are twice continuously differentiable, that is, $\mathcal{E}_\xi^a \in C^2(\mathscr{Y})$. The restricted dependence of $\mathcal{E}_\xi^a$ on atoms within the cut-off radius may also be expressed in the form

$$\frac{\partial \mathcal{E}_\xi^a}{\partial y(\eta)}(y) = 0 \text{ for all } \eta \text{ with } |y(\eta) - y(\xi)| \geq r_c.$$

This quantifies the requirement that the site-energy is localized.

Given $\mathcal{E}_\xi^a$ we define the energy of Ω subjected to y by

$$(2.4) \qquad\qquad\qquad \mathcal{E}^a(y) := \sum_{\xi \in \Omega} \mathcal{E}_\xi^a(y).$$

We call an energy of the form (2.4) where $\mathcal{E}_\xi^a$ satisfies (2.3) *homogeneous*. When we define the Cauchy–Born strain energy density corresponding to (2.4) in Section 3, we use that $\mathcal{E}^a$ is homogeneous: if $\mathcal{E}^a$ is not homogeneous, the energy per unit volume in a perfect lattice subjected to uniform strain may not be well defined.

Remark 2.1. *The locality assumption can, in principle, be replaced by an assumption that the interaction strength decays sufficiently rapidly with increasing distance between atoms.*

Remark 2.2. *Homogeneity of the site-energy is our main assumption that is violated for multi-lattices. We show in [17] how to generalize our formulation for that scenario.*

3. The Cauchy–Born Site Energy

BQCE is a coupling of an atomistic energy based on (2.4) with a coarse-grained continuum elastic energy based on the Cauchy–Born strain energy density (3.1). Let $\text{vor}(\xi)$ denote the Voronoi cell of a site $\xi \in \Lambda$. Then the Cauchy–Born strain energy density $W : \text{GL}(\mathbb{R}^d) \to \mathbb{R}$ corresponding to V is defined by

$$(3.1) \qquad\qquad\qquad W(F) := \frac{1}{|\text{vor}(0)|} \mathcal{E}_0^a(y^F),$$

where $y^F \in \mathscr{Y}$ is the homogeneous deformation $y^F(\xi) = F\xi$. $W(F)$ may be interpreted as the energy per unit volume in Λ subjected to strain F. Note that the assumption of homogeneity (2.3) ensures that $\mathcal{E}^a_\xi(y^F) = \mathcal{E}^a_0(y^F)$ for all $\xi \in \Lambda$.

We will use the Cauchy–Born strain energy density (3.1) to derive a coarse-grained continuum energy suitable for coupling with the atomistic energy (2.4). First, we define a space of coarse-grained deformations. Choose *representative atoms (repatoms)* in Λ, and let Λ^{rep} denote the set of repatoms. Let $\mathcal{T}$ be a triangulation of Λ^{rep}, and let $P^1(\mathcal{T})$ denote the set of all functions $y : \mathbb{R}^d \to \mathbb{R}^d$ that are continous and piecewise affine with respect to $\mathcal{T}$. We call $P^1(\mathcal{T})$ the set of *coarse-grained deformations*. The Cauchy–Born energy of a deformation $y \in P^1(\mathcal{T})$ in a domain Ω is then given by

$$\mathcal{E}^c(y) := \int_\Omega W(\nabla y(x))dx.$$

The Cauchy–Born approximation is analyzed, for example, in [4, 7, 10].

The definition of the QCE method [14] and our construction of the BQCE method in the next section use a Cauchy–Born site-energy $\mathcal{E}^c_\xi$, which is analogous to the atomistic site-energy $\mathcal{E}^a_\xi$. For $y \in P^1(\mathcal{T})$ and $\xi \in \Lambda$, we define $\mathcal{E}^c_\xi$ by

$$\begin{aligned}
\mathcal{E}^c_\xi(y) : &= \int_{\mathrm{vor}(\xi)} W(\nabla y(x))dx \\
&= \sum_{T \in \mathcal{T}} |\mathrm{vor}(\xi) \cap T| W(\nabla y|_T).
\end{aligned}$$
(3.2)

In formula (3.2), $|\mathrm{vor}(\xi) \cap T|$ denotes the volume of the intersection of $\mathrm{vor}(\xi)$ with the element T. We observe that the sum on the right hand side of equation (3.2) is finite because only finitely many elements $T \in \mathcal{T}$ can intersect $\mathrm{vor}(\xi)$.

4. The Blended Quasicontinuum Energy

4.1. **Formulation of the BQCE method.** The Blended Quasicontinuum Energy (BQCE) is an atomistic-to-continuum coupling based on the Quasicontinuum Energy (QCE) of Tadmor *et al.* [14]. In QCE, the reference domain Ω_a is partitioned into an atomistic region $\mathcal{A}$ and a continuum region $\mathcal{C}$, and the QC energy $\mathcal{E}^{QC} : P^1(\mathcal{T}) \to \mathbb{R}$ is defined by

$$\mathcal{E}^{QC}(y) := \sum_{\xi \in \mathcal{A}} \mathcal{E}^a_\xi(y) + \sum_{\xi \in \mathcal{C}} \mathcal{E}^c_\xi(y).$$
(4.1)

In BQCE, the atomistic and continuum energies per atom are weighted averages. Given a *blending function* $\beta : \Omega_a \to [0, 1]$ the BQCE energy $\mathcal{E}^\beta : P^1(\mathcal{T}) \to \mathbb{R}$ is defined by

$$\mathcal{E}^\beta(y) := \sum_{\xi \in \Omega_a} \beta(\xi)\mathcal{E}^c_\xi(y) + (1 - \beta(\xi))\mathcal{E}^a_\xi(y).$$
(4.2)

We observe that the QC energy with continuum region $\mathcal{C}$ is the same as the BQCE energy with β chosen as the characteristic function of $\mathcal{C}$. Our formulation of BQCE is similar in spirit to the bridging domain method [3], the AtC coupling [1], and the Arlequin method [2].

The BQCE energy can be rewritten in the form

$$\mathcal{E}^\beta(y) = \sum_{\xi \in \Omega_a} \beta(\xi) \int_{\mathrm{vor}(\xi)} W(\nabla y) \, dx + (1 - \beta(\xi)) \mathcal{E}^a_\xi(y)$$

$$= \sum_{\xi \in \Omega_a} \sum_{T \in \mathcal{T}} \beta(\xi) |\mathrm{vor}(\xi) \cap T| W(\nabla y|_T) + \sum_{\xi \in \Omega_a} (1 - \beta(\xi)) \mathcal{E}^a_\xi(y)$$

$$(4.3) \qquad = \sum_{T \in \mathcal{T}} v_T^\beta W(\nabla y|_T) + \sum_{\xi \in \Omega_a} (1 - \beta(\xi)) \mathcal{E}^a_\xi(y),$$

where the *BQCE-effective volume* of the element T is defined by

$$(4.4) \qquad\qquad v_T^\beta := \sum_{\xi \in \Omega_a} \beta(\xi) |\mathrm{vor}(\xi) \cap T|.$$

Remark 4.1. *The triangulation $\mathcal{T}$ need not cover the entire domain Ω_a. For $\mathcal{T}$ a triangulation which covers only part of $\mathbb{R}^d$, define*

$$\Omega(\mathcal{T}) := \cup_{T \in \mathcal{T}} T, \;\; and$$

$$P^1(\mathcal{T}) := \{y : \Omega(\mathcal{T}) \cup \Lambda \to \mathbb{R}^d : \; y \text{ piecewise affine w.r.t. } \mathcal{T} \text{ on } \Omega(\mathcal{T})\}.$$

We observe that $\mathcal{E}^\beta(y)$ is defined for $y \in P^1(\mathcal{T})$ if for every $\xi \in \Omega_a$ such that $\beta(\xi) > 0$ we have $\mathrm{vor}(\xi) \subset \Omega(\mathcal{T})$. In particular, it is not necessary to assume that the triangulation $\mathcal{T}$ is refined to atomistic scale anywhere in the domain Ω_a. It is possible that the use of a mesh which is not refined to atomistic scale may make the implementation of BQCE easier and more efficient in some cases.

4.2. **Far-field boundary conditions.** A typical application of the BQCE method is the simulation of a defect or defect region in an infinite crystal. To that end, we require far-field boundary conditions at the domain boundary. We propose two choices.

4.2.1. *Dirichlet boundary conditions.* Let $\mathcal{S} \subset \mathcal{T}$ be a finite subset of $\mathcal{T}$, and let $\Omega(\mathcal{S}) := \cup_{S \in \mathcal{S}} S$ be a polygonal domain. When Dirichlet boundary conditions are imposed, the deformation of the boundary $\partial\Omega(\mathcal{S})$ of $\Omega(\mathcal{S})$ is fixed to agree with some $y_0 \in P^1(\mathcal{T})$. Precisely, we let

$$(4.5) \qquad \mathrm{Adm} := \{y \in P^1(\mathcal{T}) : y(x) = y_0(x) \text{ for all } x \in \partial\Omega(\mathcal{S})\}$$

denote the space of admissible deformations. We then solve the problem

$$(4.6) \qquad\qquad \text{Find } y \in \operatorname*{argmin}_{z \in \mathrm{Adm}} \mathcal{E}^\beta(z),$$

where we interpret $\operatorname{argmin}_{z \in \mathrm{Adm}} \mathcal{E}^\beta(z)$ as the set of *local* minimizers of $\mathcal{E}^\beta$.

4.2.2. *Periodic boundary conditions.* A popular method to construct artificial far-field boundary conditions is to formulate the problem in a periodic cell. To that end, suppose that $\Omega(\mathcal{T}) = \mathbb{R}^d$, $\mathcal{T}$ is periodic, and let $\mathcal{S} \subset \mathcal{T}$ be the finite element mesh on one periodic cell. That is, suppose that there exists a matrix $A \in \mathrm{GL}(\mathbb{R}^d)$ such that

$$\mathcal{T} = \bigcup_{n \in \mathbb{Z}^d} \{An + \mathcal{S}\},$$

and that this union is disjoint.

Given a *homogeneous* far-field macroscopic strain $F \in \mathrm{GL}(\mathbb{R}^d)$, we then define the admissible set as

(4.7) $\qquad \mathrm{Adm} := \left\{ y \in P^1(\mathcal{T}) : y(x + An) = y(x) + FAn \text{ for all } x \in \mathbb{R}^d \right\}.$

The associated variational problem can again be stated as (4.6).

4.3. **Complexity and optimal parameters.** In [17], we conjecture an error estimate for BQCE in 2D and 3D. The conjecture is based on our error analysis of BQCE in 1D [23] and on the consistency estimates for BQCE in 2D and 3D in [17]. Following [16, Sec. 7.1], we use our conjectured error estimate to derive *complexity estimates*, which are bounds on the error of the BQCE method in terms of the number of degrees of freedom. We use our complexity estimates to guide the choice of optimal approximation parameters $\mathcal{T}$ and β.

Let y_a be an equilibrium of the atomistic energy, and let y_β be an equilibrium of BQCE with the same boundary conditions as y_a. Let h be the mesh size function of the triangulation $\mathcal{T}$ ($h(x) = \mathrm{diam}(T)$ for a.e. $x \in T$), and let β be the blending function. Then we conjecture an estimate of the form:

(4.8)
$$\mathrm{Err} := \|Dy_\mathrm{a} - Dy_\beta\|_{L^p} \lesssim \|hD^2y_\mathrm{a}\|_{L^p(C)} + \|D^2\beta\|_{L^p}$$
$$=: \mathrm{CG} + \mathrm{GF},$$

for all $p \in [1, \infty]$ (however, for $p \in \{1, \infty\}$, it is unclear in what generality this result may hold). In (4.8), D^2y_a and $D^2\beta$ should be interpreted as the second derivatives of smooth interpolants of y_a and β, and $C := \mathrm{supp}(\beta)$. The first term, $\mathrm{CG} = \|h\nabla^2 y_\mathrm{a}\|_{L^p(C)}$, is the finite element *coarsening error*, while the second term, $\mathrm{GF} = \|D^2\beta\|_{L^p}$, measures the effect of the ghost forces.

We now describe the problem of a point defect in a 2D crystal. To quantify the notion of a point defect, we assume that for some $\alpha > 0$,

(4.9) $\qquad |D^2y_\mathrm{a}(x)| \simeq r^{-\alpha}, \qquad \text{where } r = |x|.$

It has been observed in numerical experiments that $\alpha = 2$ for a dislocation, and that $\alpha = 3$ for a vacancy [9, 16]. We assume that the reference domain Ω is a roughly circular region of radius N atomic spacings centered at the origin. We let $K_0 > 0$ be the radius of the atomistic region surrounding the defect, and we let $K_1 > 0$ be the width of the blending region. We then choose a radial blending function β of the form

(4.10) $\qquad \beta(x) := \begin{cases} 0 & \text{if } r < K_0, \\ \beta_0\left(\frac{|x| - K_0}{K_1}\right) & \text{if } K_0 \leq r < K_0 + K_1, \\ 1 & \text{if } K_0 + K_1 \leq r, \end{cases}$

where $\beta_0 : [0, 1] \to [0, 1]$ is a twice continuously differentiable function with $\beta_0(0) = \beta_0'(0) = \beta_0'(1) = 0$ and $\beta_0(1) = 1$.

We summarize our complexity estimates for BQCE in Table 4.3. These estimates are proved in [17]. We distinguish three cases based on the value of $\gamma := \frac{\alpha p}{p+2}$. In the second column, we give the optimal rates of convergence for BQCE. The optimal rates are attained when K_1 is given in terms of K_0 by the formula appearing in the third column and when the mesh size function h is given by

(4.11) $\qquad h(x) = \left(\frac{|x|}{K_0}\right)^\gamma.$

TABLE 1. Complexity estimates and optimal approximation parameters for BQCE [17]. The estimates above are for the problem of a point defect in a two-dimensional crystal. The variables K_0, K_1, N, and α are defined in Section 4.3, and $\gamma := \frac{\alpha p}{p+2}$. In all cases, the optimal rate of convergence is attained when $h = \left(\frac{|x|}{K_0}\right)^\gamma$ and when K_1 is given in terms of K_0 by the formula in the third column above.

Case	Complexity Estimate	Optimal Parameters
$\gamma > 1$	$\|\nabla y_a - \nabla y_\beta\|_{L^p} \lesssim \mathrm{DoF}^{\max\{\frac{1}{p}-1, \frac{1}{p}-\frac{\alpha}{2}\}}$	$K_1 = K_0$
$\gamma = 1$	$\|\nabla y_a - \nabla y_\beta\|_{L^p} \lesssim \mathrm{DoF}^{\max\{\frac{1}{p}-1, -\frac{1}{2}\}}$	$K_1 = K_0 \ln\left(\frac{N}{K_0}\right)^{\frac{1}{2}}$
$\gamma < 1$	$\|\nabla y_a - \nabla y_\beta\|_{L^p} \lesssim \mathrm{DoF}^{\max\{\frac{1}{p}-1, -\frac{1}{2}\}}$	$K_1 = K_0^\gamma N^{1-\gamma}$

Remark 4.2. *The rates of convergence depend on the geometry of the problem and on the norm in which the error is measured. We observe that the error of BQCE does not decrease with* DoF *when measured in the $W^{1,1}$-seminorm. This is because the $W^{-1,1}$-norm of the ghost force does not decrease as the size of the blending region increases.*

Remark 4.3. *When α is small, the rate of convergence of BQCE is the same as the rate of convergence of Shapeev's method in some norms. In fact, if $\alpha \leq 2$ (e.g., a dislocation), then the $W^{1,2}$-error of Shapeev's method decreases as $\mathrm{DoF}^{-\frac{1}{2}}$ with the number of degrees of freedom [16]. We predict the same rate of convergence for BQCE when $\alpha \leq 2$. On the other hand, when α is larger, a patch test consistent coupling such as Shapeev's method may converge faster than BQCE. When $\alpha > 2$ (e.g., a vacancy, micro-crack, or dislocation dipole), the $W^{1,2}$-error of Shapeev's method decreases as $\mathrm{DoF}^{\frac{1}{2}-\frac{\alpha}{2}}$, whereas the $W^{1,2}$-error of BQCE decreases as $\mathrm{DoF}^{-\frac{1}{2}}$. Roughly speaking, this is because when α is small, the coarse-graining error dominates, but when α is large, the ghost force error dominates.*

5. NUMERICAL EXAMPLE

5.1. **Setup of the atomistic model.** In the 2D triangular lattice defined by

$$\Lambda := \begin{pmatrix} 1 & 1/2 \\ 0 & \sqrt{3}/2 \end{pmatrix} \cdot \mathbb{Z}^2$$

we choose a hexagonal domain Ω_a with embedded micro-crack as described in Figure 1. The sidelength of the domain is $N = 300$ atomic spacings, and a "micro-crack" is introduced by removing a segment of nine atoms $\Lambda^{\mathrm{crack}} := \{-4e_1, \ldots, 4e_1\}$ at the center of Ω_a.

The domain is supplied with periodic boundary conditions (4.7) with macroscopic strain given by

$$F := \begin{pmatrix} 1 & \gamma_{\mathrm{II}} \\ 0 & 1 + \gamma_{\mathrm{I}} \end{pmatrix} \cdot F_0,$$

where $F_0 \propto I$ minimizes the Cauchy–Born stored energy function W and $\gamma_{\mathrm{I}}, \gamma_{\mathrm{II}}$ are small loading parameters. Thus, the crack is loaded in mixed mode I & II. We solve
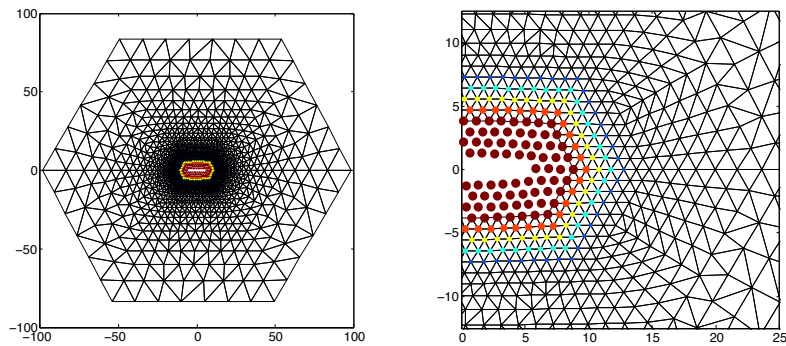
FIGURE 1. Deformed configuration in atomic units of a BQCE solution for a microcrack in a computational domain with approximately $3N^2$ atoms ($N = 100$ in this figure, but $N = 300$ in the benchmark described in Section 5.3). The color and size of the atom positions indicate the value of the blending function.

the atomistic model (for the computation of errors) in the same periodic domain in order to avoid taking into account additional approximation errors due to the choice of far-field boundary condition.

The site energy is given by the EAM toy-model (2.2), with

$$\phi(r) = \eta(r)\big[e^{-2a(r-1)} - 2e^{-a(r-1)}\big], \quad \rho(r) = \eta(r)e^{-br}, \quad \text{and}$$
$$G(\bar{\rho}) = c\big[(\bar{\rho} - \bar{\rho}_0)^2 + (\bar{\rho} - \bar{\rho}_0)^4\big],$$

where $a, b, c, \bar{\rho}_0 \in \mathbb{R}$ are parameters of the model and $\eta \in C^{2,1}(\mathbb{R})$ is a cut-off function defined through

$$\begin{cases} \eta(r) = 1, & \text{for } r < r_1^{\text{cut}}, \\ \eta(r) \in [0, 1], & \text{for } r_1^{\text{cut}} < r < r_2^{\text{cut}}, \\ \eta(r) = 0, & \text{for } r > r_2^{\text{cut}}, \end{cases}$$

and the requirement that η is a quintic polynomial in $[r_1^{\text{cut}}, r_2^{\text{cut}}]$, where $r_1^{\text{cut}}, r_2^{\text{cut}}$ are additional parameters of the model. In our computational experiment we choose

$$a = 4.4, \quad b = 3, \quad c = 5, \quad t_0 = 6e^{-b}, \quad r_1^{\text{cut}} = 1.8, \quad r_2^{\text{cut}} = 2.5.$$

5.2. **Setup of the BQCE method.** Our implementation of the BQCE method is based on (4.3), using standard finite element assembly techniques. The construction of the blending function is governed by two approximation parameters:

- $K_0 \in \mathbb{N}$ denotes the number of atomic layers surrounding the micro-crack where $\beta = 1$;
- $K_1 \in \mathbb{N}$ denotes the number of atomic layers in the blending region.

For the micro-crack problem we expect $\alpha = 3$ in the context of Section 4.3. Hence, according to Table 4.3, the choice $K_1 := K_0$ (so that the number of atoms in the atomistic region and blending region are comparable) is quasi-optimal for both $p = 2$ and $p = \infty$.

Let $d_{\text{hop}}(\xi, \eta)$ denote the hopping distance in the triangular lattice (with natural extension to sets), then we define

$$\Lambda^{\text{a}} := \big\{\xi \in \Omega_{\text{a}} : d_{\text{hop}}(\xi, \Lambda^{\text{crack}}) \leq K_0\big\}, \quad \text{and}$$

$$\Lambda^{\text{b}} := \big\{\xi \in \Omega_{\text{a}} : K_0 < d_{\text{hop}}(\xi, \Lambda^{\text{crack}}) \leq K_0 + K_1\big\}.$$

We consider three choices of the blending function, which are all easily defined for general interface geometries:

- *QCE:* choosing β to be the characteristic function of the atomistic region Λ^{a}, and $K_1 = 0$, yields the QCE method defined in (4.1).
- *Linear Blending:* Let $d(\xi)$ denote the hopping distance from the atomistic region, then we choose

$$\beta_{\text{lin}}(\xi) := \max(1, d(\xi)/K_1).$$

- *Smooth Blending:* Let $\Delta_i^2 \beta(\xi) := \beta(\xi + a_i) - 2\beta(\xi) + \beta(\xi - a_1)$, and let $\Phi(\beta) := \sum_{\xi \in \Omega_{\text{a}}} \sum_{i=1}^3 |\Delta_i^2 \beta(\xi)|^2$, then we define

$$\beta_{\text{smooth}} := \text{argmin}\big\{\Phi(\beta) : \beta(\xi) = 0 \text{ in } \Lambda^{\text{a}} \text{ and } \beta(\xi) = 1 \text{ in } \Omega_{\text{a}} \setminus \Lambda^{\text{a}} \cup \Lambda^{\text{b}}\big\}.$$

The third approximation parameter is the finite element mesh in the continuum region. We coarsen the finite element mesh away from the boundary of the blending region according to the rule suggested by the complexity estimates in Table 4.3. As a matter of fact it turns out that the mesh size growth is too rapid to create shape-regular meshes, hence we also impose the restriction that neighbouring element can at most grow by a prescribed factor; this introduces an additional logarithmic factor in the complexity estimates [16, Sec. 7.1].

The resulting energy functional is minimized using the preconditioned Polák–Ribière conjugate gradient algorithm described in [22]. We removed the termination criterion in this algorithm and allowed it to converge to its maximal precision, that is, until the numerically computed descent direction ceases to be an actual descent direction for the energy; this occurs at an accuracy of 10^{-5} to 10^{-6} in atomic units.

5.3. **Rates of Convergence.** In our numerical experiment, we choose $\gamma_{\text{I}} = \gamma_{\text{II}} = 0.03$ (3% shear and 3% tensile stretch), solve the BQCE problem (to be precise, the QCE and the BQCE problems for linear and smooth blending functions) for increasing parameters K_0, and compute the error relative to the exact atomistic solution.

The relative errors in the $W^{1,2}$-seminorm are displayed in Figure 2; the relative errors in the $W^{1,\infty}$-seminorm are displayed in Figure 3; the errors in the energy are displayed in Figure 4. We observe clear qualitative agreement with our theoretical predictions.

However, it is worth pointing out that the advantage of a smooth blending function is less pronounced than our theory might suggest. As a matter of fact, it appears that smooth blending functions only become advantageous for fairly wide blending regions. (The two last datapoints in the graphs for the BQCE methods correspond, respectively, to $K_1 = 22$ and $K_1 = 32$.

References

[1] S. Badia, M. Parks, P. Bochev, M. Gunzburger, and R. Lehoucq. On atomistic-to-continuum coupling by blending. *Multiscale Model. Simul.*, 7(1):381–406, 2008.
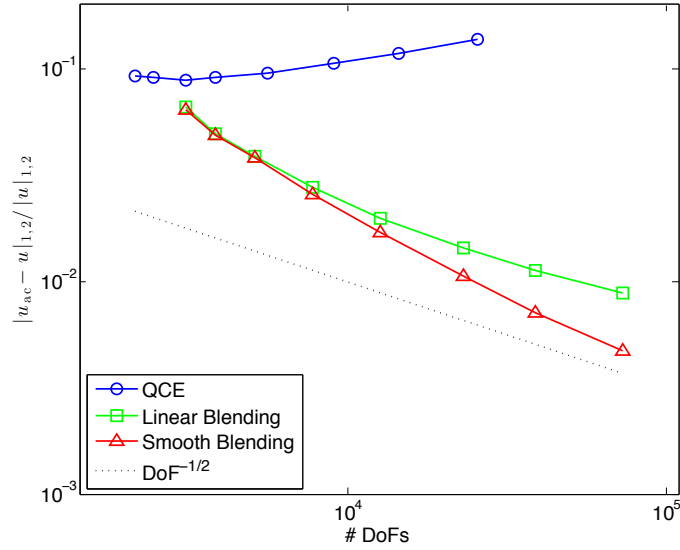
FIGURE 2. Convergence rates in the energy-norm (the H^1-seminorm) for the micro-crack benchmark problem described in Section 5.
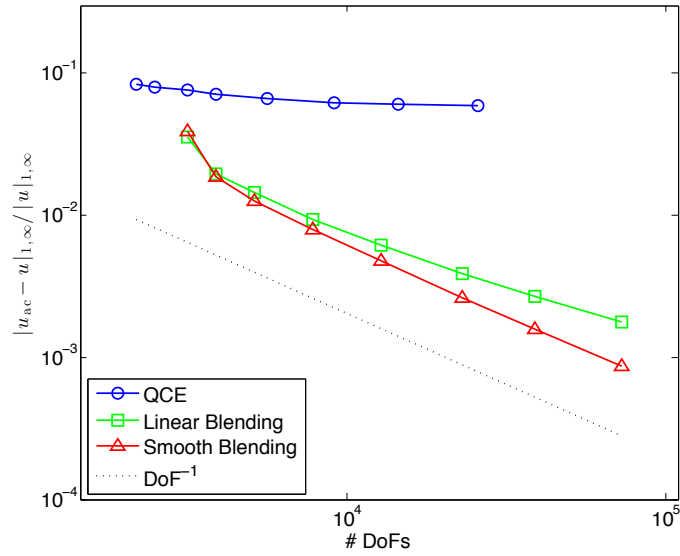

FIGURE 3. Convergence rates in the $W^{1,\infty}$-seminorm for the micro-crack benchmark problem described in Section 5.

[2] P. T. Bauman, H. B. Dhia, N. Elkhodja, J. T. Oden, and S. Prudhomme. On the application of the Arlequin method to the coupling of particle and continuum models. *Comput. Mech.*, 42(4):511–530, 2008.
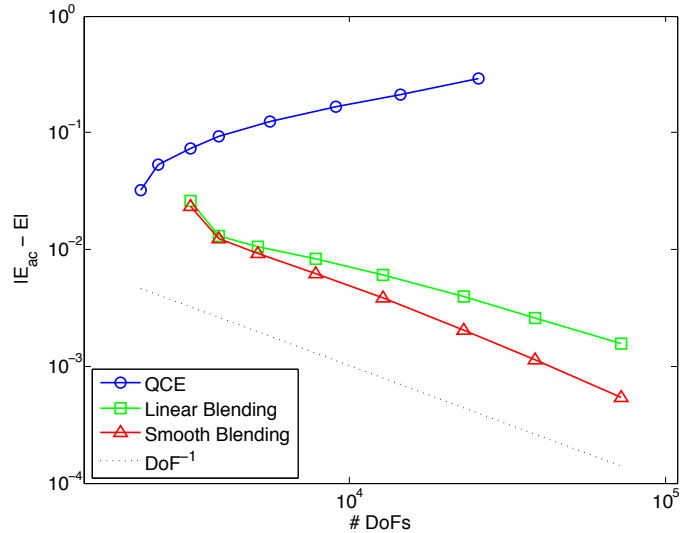
FIGURE 4.   Convergence rates in the energy, for the micro-crack
benchmark problem described in Section 5.

[3] T. Belytschko and S. P. Xiao. Coupling methods for continuum model with molecular model.
     International Journal for Multiscale Computational Engineering, 1:115–126, 2003.
[4] X. Blanc, C. Le Bris, and P.-L. Lions. From molecular models to continuum mechanics. *Arch.
     Ration. Mech. Anal.*, 164(4):341–381, 2002.
[5] L. M. Dupuy, E. B. Tadmor, F. Legoll, R. E. Miller, and W. K. Kim. Finite-temperature
     quasicontinuum. manuscript, 2011.
[6] W. E, J. Lu, and J. Yang. Uniform accuracy of the quasicontinuum method. *Phys. Rev. B*,
     74(21):214115, 2006.
[7] W. E and P. Ming. Cauchy-Born rule and the stability of crystalline solids: static problems.
     Arch. Ration. Mech. Anal., 183(2):241–297, 2007.
[8] H. Fischmeister, H. Exner, M.-H. Poech, S. Kohlhoff, P. Gumbsch, S. Schmauder, L. S.
     Sigi, and R. Spiegler. Modelling fracture processes in metals and composite materials. *Z.
     Metallkde.*, 80:839–846, 1989.
[9] F. C. Frank and J. H. van der Merwe. One-dimensional dislocations. I. static theory. *Proc.
     R. Soc. London*, A198:205–216, 1949.
[10] T. Hudson and C. Ortner. On the stability of bravais lattices and their cauchy–born approx-
     imations. *M2AN Math. Model. Numer. Anal.*, 46, 2012.
[11] M. Iyer and V. Gavini. A field theoretical approach to the quasi-continuum method. *Journal
     of the Mechanics and Physics of Solids*, 59(8):1506 – 1535, 2011.
[12] W. K. Kim, E. B. Tadmor, M. Luskin, D. Perez, and A. Voter. Hyper-qc: An accelerated
     finite-temperature quasicontinuum method using hyperdynamics. manuscript, 2011.
[13] R. Miller and E. Tadmor. A unified framework and performance benchmark of fourteen
     multiscale atomistic/continuum coupling methods. *Modelling Simul. Mater. Sci. Eng.*, 17,
     2009.
[14] M. Ortiz, R. Phillips, and E. B. Tadmor. Quasicontinuum analysis of defects in solids. *Philo-
     sophical Magazine A*, 73(6):1529–1563, 1996.
[15] C. Ortner and A. Shapeev. work in progress.
[16] C. Ortner and A. V. Shapeev. Analysis of an Energy-based Atomistic/Continuum Coupling
     Approximation of a Vacancy in the 2D Triangular Lattice. *ArXiv e-prints*, 1104.0311, Apr.
     2010.
[17] C. Ortner and B. Van Koten. Blended atomistic/continuum hybrid methods I: Formulation
     and consistency. manuscript.

[18] C. Ortner and L. Zhang. Construction and sharp consistency estimates for atomistic/continuum coupling methods with general interfaces: a 2d model problem. arXiv:1110.0168.

[19] A. Shapeev. Consistent energy-based atomistic/continuum coupling for two-body potentials in one and two dimensions. *Multiscale Model. Simul.*, 9(3):905–932, 2011.

[20] A. V. Shapeev. Consistent energy-based atomistic/continuum coupling for two-body potentials in three dimensions. arXiv:1108.2991.

[21] T. Shimokawa, J. Mortensen, J. Schiotz, and K. Jacobsen. Matching conditions in the quasicontinuum method: Removal of the error introduced at the interface between the coarse-grained and fully atomistic region. *Phys. Rev. B*, 69(21):214104, 2004.

[22] B. Van Koten, X. H. Li, M. Luskin, and C. Ortner. A computational and theoretical investigation of the accuracy of quasicontinuum methods. In I. Graham, T. Hou, O. Lakkis, and R. Scheichl, editors, *Numerical Analysis of Multiscale Problems*. Springer, to appear. arXiv:1012.6031.

[23] B. Van Koten and M. Luskin. Analysis of energy-based blended quasicontinuum approximations. *SIAM J. Numer. Anal.*, to appear. arXiv:1008.2138v3.

M. Luskin, 127 Vincent Hall, 206 Church St. SE, Minneapolis, MN 55455, USA
E-mail address: `luskin@math.umn.edu`

C. Ortner, Mathematics Institute, Zeeman Building, University of Warwick, Coventry CV4 7AL, UK
E-mail address: `christoph.ortner@warwick.ac.uk`

B. Van Koten, 127 Vincent Hall, 206 Church St. SE, Minneapolis, MN 55455, USA
E-mail address: `vankoten@math.umn.edu`